Check for updates

ADVANCED THEORY AND SIMULATIONS
www.advtheorysimul.com

Heterogeneity in Silk Piezoelectricity

Seçkin D. Günay

Experimental studies demonstrates that silk exhibits good piezoelectric properties among biological materials. It has been proven by experimenters that the material, which contains amorphous and secondary structures, acquires this property from β-sheet crystals. In this study, the piezoelectric properties of silk II β-sheets are investigated at the microscopic level. Models existing in the literature are examined using computational methods. Shear deformation is applied to these structures, and piezoelectric coefficients (d_{14}) are calculated. Two models provided by recent studies, Asakura A and B, form silk fibroin and are distributed with a 2:1 ratio. The overall piezoelectric property emerges with the contribution of both. It is determined that there is a six-fold difference between the piezoelectric coefficients of the two models. This signifies that these β-sheet crystal structure models that made up the silk has very different piezoelectric properties. Thus, the heterogeneity in the structure also exists in the piezoelectric property. Theoretically, there is a possibility to increase the silk piezoelectricity by increasing the Asakura Model A β-sheet concentration.

1. Introduction

Silk fiber has been used as an excellent textile for over several thousand years due to its tactile properties, visual brightness and durability.[1,2] It is a non-toxic and biodegradable material.[3] It has also strong mechanical properties with high tensile strength and toughness.[4–6] Therefore, it has received widespread attention within the scope of biomaterials. Over the past decades, scientists have made significant efforts to understand the mechanical properties of it. In the mid-20th century, the structure and physical properties of silk fiber were just being discovered experimentally and it was found that it had a piezoelectric property, which was an unexpected result for scientists.[7,8] Again, at that time, its structure was identified,[9] which is semi-crystalline. The origin of the piezoelectric property will gradually be revealed with these two newly discovered pieces of information. A few decades later, experiments on silk were performed again and the changes in the piezoelectric property of the silk fiber as a result of external factors (temperature, water) were examined.[10] Finally, in 2011,[11] experiments were carried out on zone-drawn uniaxial oriented silk films. Fukada[8] and Yucel et al.[11] studies shown that the magnitude of the piezoelectric constant of silk fiber is 1 and 1.5 pC/N, respectively. These data were acquired by applying shear deformation and measuring the direct piezoelectric coefficients.

Investigating the piezoelectric effect in polymers is an important research area. This phenomenon is observed in some biological materials and it is behind many biological processes.[12,13] When pressure or electric field is applied to a material, the piezoelectric effect can be observed. The non-centrosymmetry of a polymer enables the conversion between electrical charge and mechanical stress. When pressure is applied positive and negative charge centers shift. An electric field is created inside the polymer, and eventually, polarized charges are formed on the surface, which is called the piezoelectric effect. The mechanical stress (σ) applied to these materials produces an electric polarization (or potential) (D) (direct piezoelectric effect). Contrarily, the applied electric field (E) produces a deformation (strain) in the material (ϵ) (inverse piezoelectric effect). These two events are expressed mathematically by two linear equations, $D = d \cdot \sigma$ and $\epsilon = d \cdot E$, respectively. Here d is the piezoelectric tensor.[14]

The effects of molecular structure on piezoelectric properties are indisputable. Copolymer silk fibroin possesses a heavy chain, light chain, and glycoprotein P25. Heavy and light chains are linked together with disulfide bridges, and these are connected to the glycoprotein with non-covalent interactions. Silk fibroin has amino acids with a composition of 45.9% glycine (Gly), 30.3%, alanine (Ala), 12.1% serine (Ser), 5.3% tyrosine (Tyr), 1.8% valine. The remaining 4% consists of other amino acids.[15] Silk II form, which is the structure after spinning, possesses β-sheets. Amino acid chains are arranged in a certain order within this secondary structure. The classical pattern for this segment is the $(GA)_n$ amino acid repeat. The structure had been confirmed by many experimenters as an antiparallel β-sheet.[9,16–19] However, it has been debated whether it had a polar or antipolar structure. Studies in recent years have resulted in a consensus that it is antipolar. More importantly, it has been found that this antipolar and antiparallel structure has two different forms, that is, the β-sheet has a heterogeneous structure, and it is in the ratio of 2:1.[18,19] These structural findings will have important implications on piezoelectricity in this study.

Experimental studies depicted that to investigate silk piezoelectricity thoroughly, it was necessary to increase the β-sheet concentration with methanol treatment. However, it was

S. D. Günay
Department of Physics
Faculty of Science
Yıldız Technical University
Esenler, İstanbul 34210, Turkey
E-mail: sgunay@yildiz.edu.tr

The ORCID identification number(s) for the author(s) of this article can be found under https://doi.org/10.1002/adts.202401461

DOI: 10.1002/adts.202401461

 © 2025 Wiley-VCH GmbH

emphasized that this alone was not sufficient and that zone drawing was also required to ensure that they all aligned in a certain direction.[11,13] Thus, there is a direct relationship between silk piezoelectricity with β-sheet concentration and orientation. For this reason, this fundamental structure that creates the piezoelectric effect will be examined in this study.

2. Methods

The molecular dynamics simulation program utilized in this work is GROMACS 2024.1 version.[20–22] CHARMM force fields (CHARMM27) were used for interatomic interactions.[23] Coordinates of the silk II model (silk structure after spinning) β-sheet crystals were acquired from Marsh et al.[9] and Asakura et al.[19] studies. Marsh et al.[9] identified the crystal region as a regular array of antiparallel β-sheets. Almost half a century later, Asakura proposed a new model, which had a heterogeneous structure. There were two packing arrangements A and B. The data in these articles were used while preparing the simulation supercells. The preparation process was described in Section S1 (Supporting Information). In the present study, the chain orientations of the original studies were preserved for all three models. The chain orientation of the Marsh Model in the original study is y. They were z for the Model A and y for the Model B in the study of Asakura. In these directions, both ends of the polymer strands were connected, and the "periodic_molecules" command of GROMACS was used. A periodic boundary condition was also implemented to MD supercells, thus creating infinite β-sheet crystal structures. Thus, it was provided for both bonded and non-bonded interactions. Non-bonded van der Waals interaction was calculated using a cutoff for neighbor lists at 1.2 nm. A switching function was used that smoothly reduces the strength to zero between 1.0 and 1.2 nm. The electrostatic interactions were computed by the Particle-Mesh Ewald (PME) model with a cutoff of 1.2 nm. The equilibrium simulation process has three steps. The first step was energy minimization using the steepest descent method. Thus, non-physical configurations were eliminated. Minimization was stopped when the maximum force was below 1 kJ/(mol.nm). Energy-minimized coordinates and topology files were given as zip file in Supporting Information. In the second step, NVT simulation was initiated at 300 K temperature. A velocity rescaling algorithm was used in this part, which lasted 10 ns. The simulation time step interval was 1fs. Position restraint was applied to all atoms other than hydrogen. A leap-frog algorithm was used for integrating Newton's equations of motion. In the third step, an NPT ensemble was initiated and an anisotropic Berendsen barostat was implemented at 1 bar pressure while keeping the temperature at 300 K. Again, position restraint and velocity rescaling algorithms were applied to the system for 10 ns. An accurate thermodynamic ensemble had not been obtained with this method, but equilibrium can be achieved efficiently. Thus, the equilibration process was completed. In the following step, fourth, the process of obtaining and processing the data was launched. An NPT ensemble was applied for 50 ns. The Parrinello–Rahman barostat, which is a more accurate pressure coupling than the previous one, was performed. Position restraint on particles had been removed. The pressure coupling type was anisotropic. Data, e.g. lattice parameters, were collected for the equilibrium state and were compared with experimental data in Section 3.1. Then, fifth step, the non-equilibrium simulation process was established and mechanical loading was applied to the simulation cell. Shear stress was implemented to the simulation cell surface, which was perpendicular to the chain direction axis. This was achieved using the "deform" command in GROMACS and combined with anisotropic simulation. The velocity of deformation was 0.00005 nm/ps. This can be considered extremely "slow" and the total applied time was 20 ns. Visualizations of the shear simulations for each supercell was given in Section 2.2.1. Periodicity persisted for bonded and non-bonded interactions. Finally, all steps were carried out at room temperature (300 K). Data related to the calculation of piezoelectric properties were collected.

Table 1. The lattice parameters were measured from simulations (this work) and experiments. (C.D.: Chain Direction).

	x [Å]	y [Å]	z [Å]
MM (Sim.)	9.59	7.03 (C.D.)	8.98
AMA (Sim.)	9.49	9.23	6.98 (C.D.)
AMB (Sim.)	9.45	6.95 (C.D.)	9.69
Marsh (Exp.)[9]	9.40	6.97 (C.D.)	9.20
Takahashi (Exp.)[18]	9.38	9.49	6.98 (C.D.)

3. Results and Discussion

3.1. Lattice Constant

Before applying any deformation to the simulation box models, the equilibrium states of the simulation boxes were compared with the experimental data. Thus, it could be understood that the simulation process was working properly, supercells were stable, and had reached equilibrium. The lattice constant is one of the most important data for such a circumstance. Input data for supercells, Marsh Model (MM), Asakura Model A (AMA), and Asakura Model B (AMB), were constructed with the atomic positions given in experimental works, and the original studies remained faithful. As a result, the chain orientations formed in the simulation supercell in our study differ within themselves. In **Table 1**, data were obtained as a result of the procedures explained in the "Methods." There were experiments of lattice parameter measurements in the literature.[9,18] When the experimental and simulation measurements were compared, "*the x direction*" and "*the chain direction*" data were in good agreement. The presence of covalent bonds in the chain direction disclosed the reason for the agreement in this direction. The third lattice constant value had more volatile data. This lattice constant is in the direction of the normal of β-sheet layer and volatility was present among both simulations and experiments. The graphs and detailed explanations of the data given in this part were in Section S2 (Supporting Information).

3.2. Piezoelectric Property

$\vec{D}$, the electric displacement vector, is approximately equal to the dipole moment density (or called polarization) when the external electric field is zero.[24]

© 2025 Wiley-VCH GmbH

25130390, 2025, 7, Downloaded from https://advanced.onlinelibrary.wiley.com/doi/10.1002/adts.202401461 by Yildiz Teknik University, Wiley Online Library on [22/07/2025]. See the Terms and Conditions (https://onlinelibrary.wiley.com/terms-and-conditions) on Wiley Online Library for rules of use; OA articles are governed by the applicable Creative Commons License

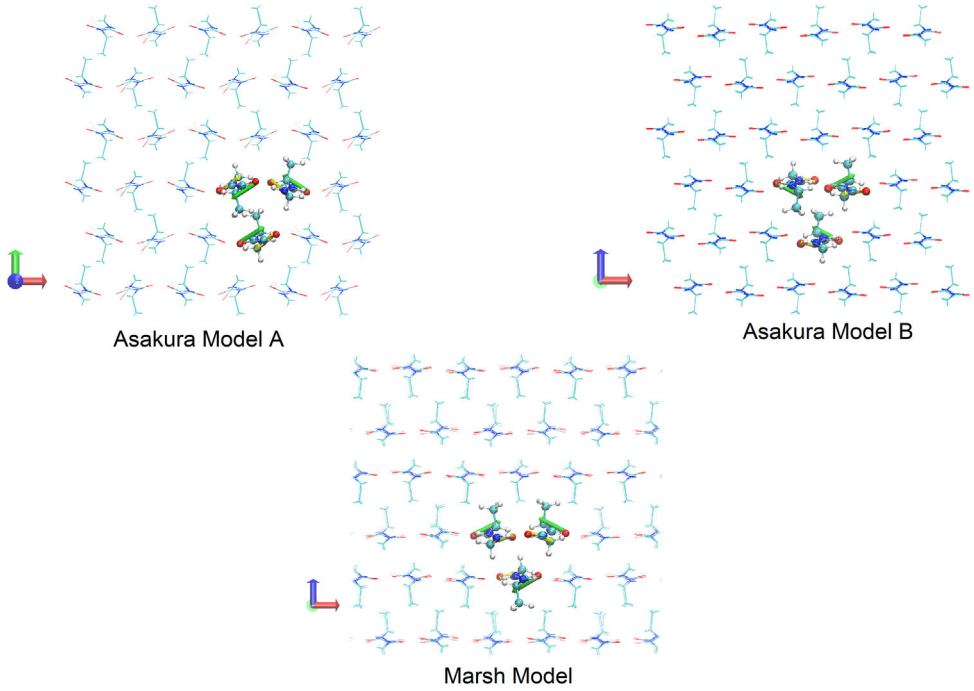


Figure 1. Models were shown along the chain direction. Dipole moment vectors of some glycine and alanine amino acids in various strands were computed and visualized by the VMD program.[25] They were represented in yellow and green arrows, respectively. See Movie S1–S3 (Supporting Information), for 3D views.

$$\vec{D} = \epsilon_0 \vec{E} + \vec{P} \tag{1}$$

$$D_i \approx P_i = \frac{p_i}{V} \tag{2}$$

Here P_i is the dipole moment density, p_i is the dipole moment of the simulation supercell, V is the volume and "i" is the i th component of vectors. Unlike most polymer structures, precise calculation of the dipole moment density was possible because the volume, which is a monoclinic β-pleated sheet silk fibroin crystal structure, was well defined.

$$p_i = \sum\nolimits_{\alpha} p_{i\alpha} \tag{3}$$

Sum over all dipole moments, $p_{i\alpha}$, of dipoles provided the dipole moment of each silk model. In this study, which was conducted using the molecular dynamics simulation method, to observe the direct piezoelectric coefficient, a mechanical stress was applied to the system and the resulting dipole moment was calculated. When stress was applied, a change from the initial state to the final state of the structure took place. This corresponds to the delta expression in the equation. The constitutive equation used for the calculations was,

$$\Delta D_i = d_{ikl}\, \Delta\sigma_{kl} \tag{4}$$

ΔD_i is introduced as the change in the polarization, $\Delta\sigma_{kl}$ is the change in the stress tensor and d_{ikl} is the direct piezoelectric coefficient. Stress components in general form are $\sigma_x, \sigma_y, \sigma_z, \sigma_{yz}, \sigma_{xz}, \sigma_{xy}$ and the corresponding subscripts are 1, 2, 3, 4, 5, 6. Polarization components are D_x, D_y, D_z and the corresponding subscripts are 1, 2, 3. The matrix of piezoelectric coefficients is as follows,

$$\begin{pmatrix} d_{11} & d_{12} & d_{13} & d_{14} & d_{15} & d_{16} \\ d_{21} & d_{22} & d_{23} & d_{24} & d_{25} & d_{26} \\ d_{31} & d_{32} & d_{33} & d_{34} & d_{35} & d_{36} \end{pmatrix} \tag{5}$$

The original orientations of structures proposed by Asakura and Marsh were different from each other. The chain direction for the AMA was z. And the chain directions for the AMB and MM were y. The constitutive equation for the early one was $\Delta D_3 = d_{36}\, \Delta\sigma_6$ and for the latter ones were $\Delta D_2 = d_{25}\, \Delta\sigma_5$. The indices of the coefficients to be attained were different. If the chain direction of all beta-sheet structures were transformed to the x direction, the equations would yield $\Delta D_1 = d_{14}\, \Delta\sigma_4$. So, they were essentially the same thing in meaning $d_{14} = d_{25} = d_{36}$. Thus, they will all be referred as d_{14}.

3.2.1. Stress and Polarization

Simulation box models and the dipole moments of some sample glycine and alanine amino acids were presented in **Figure 1**. These boxes were exposed to shear, which were perpendicular to the chain direction of the polymers. The velocity of deformation was 0.00005 nm/ps. The applied shear stress value (σ_{kl}) versus time graph was given in **Figure 2**a–c. The data fluctuates with a positive slope. At some point abruptly dropped to zero because some β-strands jumped to equilibrium positions at adjacent sites (See Section S3 and Movie S4–S6, Supporting Information). The discontinuous graphs indicated the reduction of pressure on β-strands. The most important factor was found to be the methyl

© 2025 Wiley-VCH GmbH

25130390, 2025, 7, Downloaded from https://advanced.onlinelibrary.wiley.com/doi/10.1002/adts.202401461 by Yildiz Teknik University, Wiley Online Library on [22/07/2025]. See the Terms and Conditions (https://onlinelibrary.wiley.com/terms-and-conditions) on Wiley Online Library for rules of use; OA articles are governed by the applicable Creative Commons License

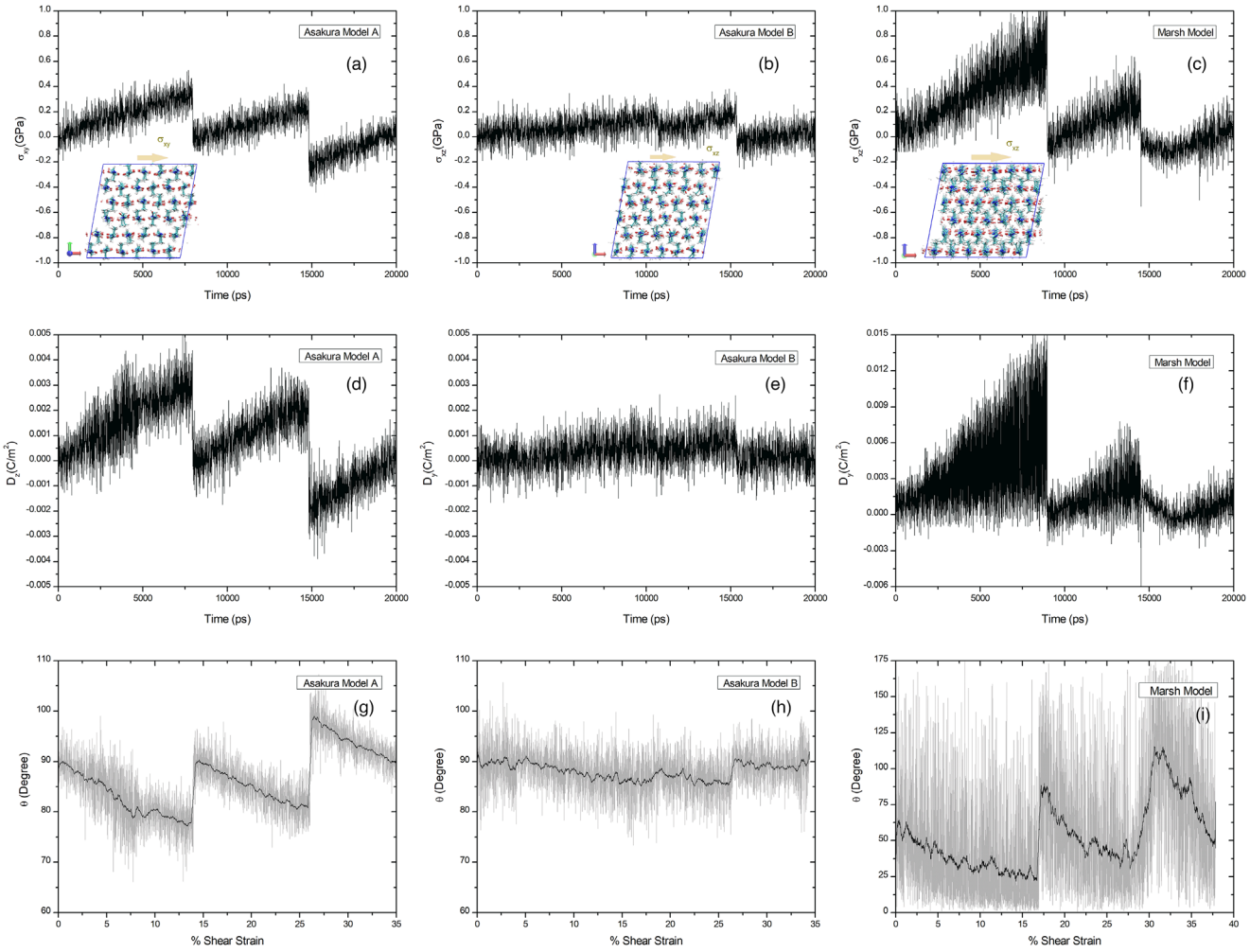


Figure 2. Applied shear stresses versus time were displayed for AMA a) AMB b) and MM c). Axial component of polarizations versus time were demonstrated for AMA d) AMB e), and MM f). Angles between total polarizations and axial polarization components versus shear strain for AMA g) AMB h), and MM i) were presented.

groups, which create a kind of "friction" due to inter-layer interaction when shear stress was applied. They cause rough spattering when released from residues positioned opposite them. AMA and MM showed significant stress responses when deformed, while little change occurred in AMB. This data was in correlation with the calculated mass densities (See Section S2, Supporting Information). The denser β-structure that underwent deformation demonstrated more stress response.

The change in polarization (dipole moment density) was investigated by applying shear stress. When all three polarization components were examined, the only component that correlated with the shear stress value was the component in the chain direction (axial component), which was perpendicular to the shear stress direction for all three models (z for AMA, y for AMB, and MM). The axial components of polarizations versus time graphs were shown in the Figure 2d–f. The increase in the applied stress caused an increase, and the subsequent rapid decrease of applied stress caused a rapid decrease in axial polarization component within the β-structure, which means a correlation. From a microscopic point of view, the methyl groups of alanine were bent as a result of shear strain. This motivated a change in the direction of their dipole moments and the total dipole moment. After the jump, they returned to their original state (see Section S4, Supporting Information)

A pronounced increase in the applied stress values caused a strong response in polarization (AMA and MM), and naturally a poor increase caused a weak response (AMB). The reactions of models, like the change in axial polarization component per unit shear stress, were not the same. To quantify the relationship between them, it is necessary to calculate the shear piezoelectric coefficient, which was calculated in the following section. The Figure 2g–i displays angles between total polarizations and fiber axes polarization components. The adjacent-averaging method was applied to the oscillating graphic data shown in gray, and results were represented in black. The angles decreased with increasing shear strain. The total polarization vectors were leaned toward the fiber axes. As the strands jump to the adjacent positions, the angles recovered almost to their initial values (See 3D vector of AMA in Movie S7 and Section S3, Supporting Information).

© 2025 Wiley-VCH GmbH

25130390, 2025, 7, Downloaded from https://advanced.onlinelibrary.wiley.com/doi/10.1002/adts.202401461 by Yildiz Teknik University, Wiley Online Library on [22/07/2025]. See the Terms and Conditions (https://onlinelibrary.wiley.com/terms-and-conditions) on Wiley Online Library for rules of use; OA articles are governed by the applicable Creative Commons License

25130390, 2025, 7, Downloaded from https://advanced.onlinelibrary.wiley.com/doi/10.1002/adts.202401461 by Yildiz Teknik University, Wiley Online Library on [22/07/2025]. See the Terms and Conditions (https://onlinelibrary.wiley.com/terms-and-conditions) on Wiley Online Library for rules of use; OA articles are governed by the applicable Creative Commons License

3.2.2. Piezoelectric Coefficient

The crystal structure has a profound effect on piezoelectricity, so understanding the configuration, orientation, and distribution of the β-crystal structure in silk is vital. Marsh et al.[9] mentioned a single type of β-crystal structure in their study, which had the form of antiparallel-chain pleated sheets and all methyl groups pointing in the same direction (polar arrangement). Three decades later, two types of β-crystal structures were found with different relative orientations, and their ratio was statistically 2:1.[18] Later studies[19] demonstrated this heterogeneous structure, and the crystal structures were concretely presented with numerical data. These antiparallel structures have two alternative antipolar arrangements. While the crystal structures were reported, experiments on piezoelectricity were performed by other groups. The shear piezoelectric coefficient of zone-drawn silk film was measured by experimenters.[11] These oriented samples displayed $d_{14} = -1.5$ pC/N. Although methanol was applied to samples, which increased the crystallinity (β-sheet content), there was no significant change in the value.[11] However, zone drawing[11] and electrical poling[26] were more effective, which were responsible for the crystal orientation.

In this study, shear piezoelectric coefficients were attained, which reveal the relationship between the polarization component and applied shear stress data, from Equation (4). The graphs were shown in **Figure 3**. Data were distributed around a linear trend, and slopes calculated from these were examined. MM had the highest value among the three structures ($d_{14} = 8.67$ pC/N). Although this model is quite old and different models have been put forward later, it was examined in this study. The more recent Asakura Models provided interesting data. The Model A value ($d_{14} = 7.16$ pC/N) is as high as the MM, while the Model B ($d_{14} = 1.19$ pC/N) is one-sixth of it. In other words, just as there is a structural heterogeneity, there is also a heterogeneity in piezoelectric coefficients. In addition, the relationship between the mass density and shear stress values mentioned above also existed with the piezoelectric coefficient. High-density β-sheet crystals had large piezoelectric coefficients. Such that, while dense structures were subjected to shear strain, more shear stress and dipole moment changes developed in the interlayer residues (see Section S4, Supporting Information). Finally, considering the 2:1 concentration ratio of Model A and Model B, roughly the mean value ($d_{14} = 5.17$ pC/N) is expected to be close to the Model A data. The findings in **Table 2** could not be directly compared with empirical data because the experimental result was for the semi-crystalline structure. Namely, there were amorphous regions as well as β-crystal structures. Moreover, although the silk film was drawn in one direction in the experiment, the orientations of the β-crystal structures were distributed around a certain angle.[11] So, it was difficult to compare with experimental data due to both the presence of amorphous structures and crystal orientation. It could be concluded that these reduce the piezoelectric properties. However, it is clear that there was a polarization response while the shear stress was applied, (d_{14}), which is consistent with the experimental data.

Table 2. The shear piezoelectric coefficient data calculated in this work and the experimental measurement were listed. The absolute value of experimental data was compared with results (see Section S5, Supporting Information for the discussion).

	AMA	AMB	MM	Experiment [semi-crystalline][11]
d_{14} (pC/N)	7.16	1.19	8.67	1.5

4. Conclusion

Experimental data showed that there was a strong relationship between shear piezoelectricity and β-sheet concentration. Although the abundance of β-sheet structures contributes to piezoelectricity, a pronounced polarization does not occur as a result of their random distribution. For this reason, the uniaxial orientation of crystal domains ensures an apparent polarization. In this context, Yucel et al.[11] stated that their results demonstrate intrinsic silk shear piezoelectricity could be explained based on overall β-sheet content and uniaxial molecular alignment. These were achieved by methanol treatment and zone drawing methods, respectively. Accordingly, in this study, silk II β-sheet models were examined and their shear piezoelectric properties were discussed. Stress, polarization component, and polarization vector changes were investigated with shear deformation. There was only one polarization component associated with the shear stress increase when shear deformation was applied. This was the axial component, which was perpendicular to the applied stress. This incident is in agreement with experimental studies. Thus, the piezoelectric coefficients (d_{14}) of the models were calculated. Interesting results were obtained by comparing the "old" model (MM) with the "new" models (AMA and AMB). Apart from the MM, AMA-AMB were found together in silk and it was shown that they were distributed with a ratio of 2:1.[11] In other words,

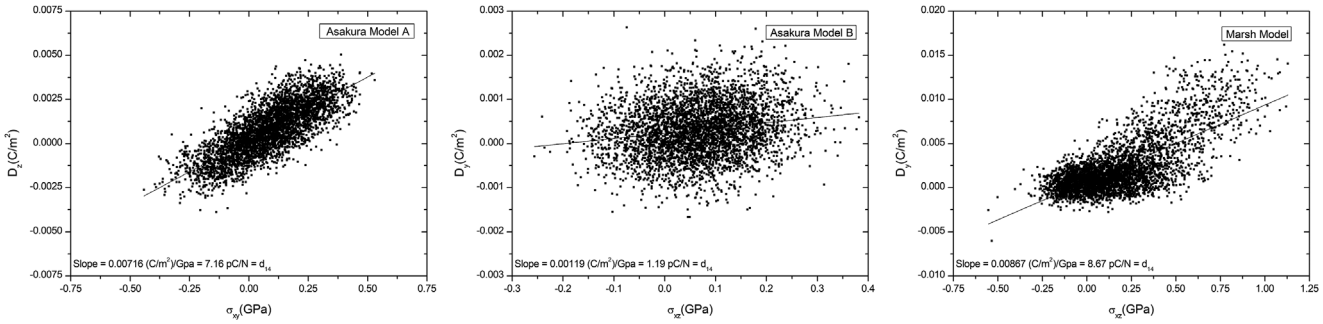


Figure 3. Axial components of polarizations of β-sheet crystal structures versus shear stresses applied perpendicular to polymer axes for AMA a) AMB b) and MM c).

 © 2025 Wiley-VCH GmbH

the Marsh Model introduced a homogenous, while the Asakura Model (also called the "Takahashi Model"[19]) put forward a heterogeneous distribution. Therefore, the average was taken according to the distribution when calculating the overall piezoelectric properties for the Asakura Model. Normally, one would expect models to have similar piezoelectric coefficients, such as MM and AMA displayed similar results. However, calculations exposed that this was not the case for AMA and AMB, that there was a six-fold difference between them. This was explained by the β-sheet crystal densities. It was argued that more compact structures were subjected to more stress due to shear strain and demonstrated more changes in the axial dipole moment vector. Methyl group of alanine exposed to stress played an important role. Still, the difference between AMA and AMB is an issue that needs to be discussed. The difference in coefficients shows us that "theoretically" it is possible to amplify the silk piezoelectric property by increasing AMA concentration. Results display that it is possible to enhance it by 38%. This could be utilized in future experimental studies alongside the methanol treatment, zone drawing, electric poling, and strong magnetic field alignment methods used to enhance silk piezoelectricity.

Supporting Information

Supporting Information is available from the Wiley Online Library or from the author.

Acknowledgements

The numerical calculations reported in this paper were partially performed at TUBITAK ULAKBIM, High Performance and Grid Computing Center (TRUBA resources). This work was supported by Yildiz Technical University Scientific Research Projects Coordination Unit under project number FBA-2024-6320.

Conflict of Interest

The authors declare no conflict of interest.

Data Availability Statement

The data that support the findings of this study are available in the supplementary material of this article.

Keywords

dipole moment, β-sheet, piezoelectric coefficient, silk

Received: December 11, 2024
Revised: February 23, 2025
Published online: March 18, 2025

[1] S. Ling, D. L. Kaplan, M. J. Buehler, *Nat. Rev. Mater.* **2018**, *3*, 18016.
[2] J. L. Yarger, B. R. Cherry, A. Van Der Vaart, *Nat. Rev. Mater.* **2018**, *3*, 18008.
[3] A. Veronica, I. M. Hsing, *ChemPhysChem* **2021**, *22*, 2266.
[4] C. Vepari, D. L. Kaplan, *Prog. Polym. Sci.* **2007**, *32*, 991.
[5] L. D. Koh, Y. Cheng, C. P. Teng, Y. W. Khin, X. J. Loh, S. Y. Tee, M. Low, E. Ye, H.-D. Yu, Y.-W. Zhang, M. Y. Han, *Prog. Polym. Sci.* **2015**, *46*, 86.
[6] A. Reizabal, C. M. Costa, L. Pérez-Álvarez, J. L. Vilas-Vilela, S. Lanceros-Méndez, *Adv. Funct. Mater.* **2023**, *33*, 2210764.
[7] E. N. Harvey, *Science* **1939**, *89*, 460.
[8] E. Fukada, *J. Phys. Soc. Jpn.* **1956**, *11*, 1301A.
[9] R. E. Marsh, R. B. Corey, L. Pauling, *Bioch. Biophys. Acta* **1955**, *16*, 1.
[10] Y. Ando, R. Okano, K. Nishida, S. Miyata, E. Fukada, *Rep. Prog. Polym. Phys. Jpn.* **1980**, *23*, 775.
[11] T. Yucel, P. Cebe, D. L. Kaplan, *Adv. Funct. Mater.* **2011**, *21*, 779.
[12] E. Fukada, *Biorheology* **1968**, *5*, 199.
[13] E. Fukada, *Ferroelectrics* **1984**, *60*, 285.
[14] R. E. Newnham, *Properties of Materials: Anisotropy, Symmetry, Structure*, Oxford University Press, New York **2005**.
[15] C. Z. Zhou, F. Confalonieri, M. Jacquet, R. Perasso, Z. G. Li, J. Janin, *Proteins: Struct., Funct., Bioinf.* **2001**, *44*, 119.
[16] S. A. Fossey, G. Némethy, K. D. Gibson, H. A. Scheraga, *Biopolym.: Orig. Res. Biomol.* **1991**, *31*, 1529.
[17] B. Lotz, F. C. Cesari, *Biochimie* **1979**, *61*, 205.
[18] Y. Takahashi, M. Gehoh, K. Yuzuriha, *Int. J. Biol. Macromol.* **1999**, *24*, 127.
[19] T. Asakura, T. Ohata, S. Kametani, K. Okushita, K. Yazawa, Y. Nishiyama, K. Nishimura, A. Aoki, F. Suzuki, H. Kaji, A. S. Ulrich, M. P. Williamson, *Macromolecules* **2015**, *48*, 28.
[20] H. J. Berendsen, D. Van Der Spoel, R. Van Drunen, *Comput. Phys. Commun.* **1995**, *91*, 43.
[21] E. Lindahl, B. Hess, D. Van Der Spoel, *J. Mol. Model.* **2001**, *7*, 306.
[22] D. Van Der Spoel, E. Lindahl, B. Hess, G. Groenhof, A. E. Mark, H. J. Berendsen, *J. Comput. Chem.* **2005**, *26*, 1701.
[23] A. D. MacKerell Jr., D. Bashford, M. Bellott, R. L. Dunbrack Jr., J. D. Evanseck, M. J. Field, S. Fischer, J. Gao, H. Guo, S. Ha, D. Joseph-McCarthy, L. Kuchnir, K. Kuczera, F. T. K. Lau, C. Mattos, S. Michnick, T. Ngo, D. T. Nguyen, B. Prodhom, W. E. Reiher, B. Roux, M. Schlenkrich, J. C. Smith, R. Stote, J. Straub, M. Watanabe, J. Wiórkiewicz-Kuczera, D. Yin, M. Karplus, *J. Phys. Chem. B* **1998**, *102*, 3586.
[24] D. J. Griffiths, *Introduction to Electrodynamics*, 3rd ed., Prentice Hall Inc., Upper Saddle River, NJ **1999**.
[25] W. Humphrey, A. Dalke, K. Schulten, *J. Mol. Graphics* **1996**, *14*, 33.
[26] V. Sencadas, C. Garvey, S. Mudie, J. J. Kirkensgaard, G. Gouadec, S. Hauser, *Nano Energy* **2019**, *66*, 104106.

 © 2025 Wiley-VCH GmbH

25130390, 2025, 7, Downloaded from https://advanced.onlinelibrary.wiley.com/doi/10.1002/adts.202401461 by Yildiz Teknik University, Wiley Online Library on [22/07/2025]. See the Terms and Conditions (https://onlinelibrary.wiley.com/terms-and-conditions) on Wiley Online Library for rules of use; OA articles are governed by the applicable Creative Commons License